



Article

Hydrogen Effect on the Cyclic Behavior of a Superelastic NiTi Archwire

Rihem Sarraj ¹, Amir Kessentini ^{2,3}, Tarek Hassine ¹, Ali Algahtani ^{2,4} and Fehmi Gamaoun ^{2,*}

¹ Laboratory of Mechanics of Sousse, National Engineering School of Sousse, University of Sousse, Sousse 4054, Tunisia; Riheme.Sarraj@eniso.rnu.tn (R.S.); tarekhassine007@gmail.com (T.H.)

² Department of Mechanical Engineering, College of Engineering, King Khalid University, Abha 61421, Saudi Arabia; akessentini@kku.edu.sa (A.K.); alialgahtani@kku.edu.sa (A.A.)

³ Laboratory of Electromechanical Systems (LASEM), National Engineering School of Sfax, University of Sfax, Route de Soukra km 4, Sfax 3038, Tunisia

⁴ Research Center for Advanced Materials Science (RCAMS), King Khalid University, PO Box 9004, Abha 61413, Asir, Saudi Arabia

Received: 13 February 2019; Accepted: 7 March 2019; Published: 11 March 2019



Abstract: In this work, we are interested in examining the strain rate effect on the mechanical behavior of Ni–Ti superelastic wires after hydrogen charging and ageing for 24 h. Specimens underwent 50 cycles of loading-unloading, reaching an imposed deformation of 7.6%. During loading, strain rates from 10^{-4} s^{-1} to 10^{-2} s^{-1} were achieved. With a strain rate of 10^{-2} s^{-1} , the specimens were charged by hydrogen for 6 h and aged for one day showed a superelastic behavior marked by an increase in the residual deformation as a function of the number of cycles. In contrast, after a few number of cycles with a strain rate of 10^{-4} s^{-1} , the Ni-Ti alloy archwire specimens fractured in a brittle manner during the martensite transformation stage. The thermal desorption analysis showed that, for immersed specimens, the desorption peak of hydrogen appeared at 320 °C. However, after annealing the charged specimens by hydrogen at 400 °C for 1 h, an embrittlement took place at the last cycles for the lower strain rates of 10^{-4} s^{-1} . The present study suggests that the embrittlement can be due to the development of an internal stress in the subsurface of the parent phase during hydrogen charging and due to the creation of cracks and local zones of plasticity after desorption.

Keywords: hydrogen; NiTi alloys; superelastic; martensite; cyclic effect

1. Introduction

The NiTi shape memory alloy (SMA) is considered as a smart material thanks to its thermomechanical behavior, such as the mechanical shape memory effect (SME) and the thermal effect (TE) [1,2], which make this alloy suitable for aerospace and Micro-Electro-Mechanical Systems industries [3]. In particular, the equiatomic NiTi SMA has been successfully used in various areas, like cardio stents, orthopedic implants and orthodontic devices, because they process, in addition to good corrosion resistance and biocompatibility with the human body, remarkable high strain recovery [4–6]. At present, superelastic NiTi alloys are extensively used for initial teeth alignment because they apply a physiological appropriate light continuous force to move the teeth to the ideal profile after few months of service life in the oral cavity [7]. Superelastic NiTi wires, in the austenitic active alloy phase, undergo a martensitic transformation phase either by temperature change or stress application [8,9]. In monotonic tensile tests, this superelasticity is manifested by a flat or nearly flat plateau in the stress-strain diagram indicating a reversible transformation from an austenite parent phase B2 to a monoclinic B19' martensite phase. Different techniques have been used to characterize

this superelastic phase transformation. In fact, C. Bewerse et al. [10] showed that the progression of the phase transformation could be identified using a 2-D digital image correlation (DIC) and would generate displacement and strain field maps of a surface by applying search and track algorithms to digital images captured during specimen deformation. Thermoelastic stress analysis (TSA) was also used to measure the stress field of loaded NiTi devices [11]. This nondestructive technique was based on detecting the increase in the stress in the local phase transformation by measuring the rise in thermoelastic signals, using a highly sensitive infrared detector. D. Delpueyo et al. [12] revealed the martensitic microstructure by infrared thermography (IRT). This technique is based on the analysis of temperature variations, measured by IRT, of the martensitic transformation during monotonic and cyclic loadings.

One of the limitations in the engineering application of the NiTi SMA is the degradation of the mechanical properties when subjected to cyclic loading. In fact, after loading and unloading, the martensite variants become wider in the plateau of martensite transformation, and the dislocation density increases [13,14]. As a consequence, the residual stain at zero stress becomes more important and the hysteresis loop area of loading and unloading decreases. G. Helbert et al. [13], indicated that after a few number of cycles, the NiTi alloy would reach stabilization in the residual strain and the maximal dissipation capacity. However, Dayananda et al. [15] showed that the dissipated energy went down with the rise in the number of cycles, and this energy increases with the growing number of cycles. Moreover, the same authors demonstrated that the dissipated energy was strongly related to the imposed strain rates. This result was in coherence with the work done by Nasser et al. [16], who inferred that the superelasticity of the NiTi alloys was very sensitive to the temperature as well as to the strain rate. Tobushi et al. [17] found that theoretical stress for martensitic transformation and the recoverable strain energy density was strongly dependent on the imposed strain rate.

On top of that, the environment has an important effect on the mechanical behavior of NiTi archwires in the oral cavity. Indeed, the diffusion of hydrogen reduces the ductility of the archwires and causes a premature fracture [18]. This hydrogen is mainly produced by the fluoride acid, which is contained in toothpastes and prophylactic agents [19–21]. After a few hours of a cathodic hydrogen charging, the superelastic NiTi SMA is fractured in the plateau of the austenite-martensite transformation [22,23]. The embrittlement of the archwire, after immersion in NaCl 0.9%, is found to be strongly related to the stress-induced martensite transformation when the amount of absorbed hydrogen is higher than 200 ppm [24,25]. This behavior is attributed to the trapped hydrogen in the defects of the NiTi alloy, which acts as a barrier for the transformation of the parent phase to the martensite phase [26,27].

In monotonic tensile tests, the embrittlement of the NiTi alloy strongly depends on the imposed strain rate [28–30]. In fact, after 8 h of hydrogen charging with a current density of 10 A/m², an embrittlement occurred for strain rates higher than 10⁻³ s⁻¹, whereas no embrittlement is detected lower than 10⁻⁴ s⁻¹. This behavior is attributed to the interaction between the higher diffused quantity of hydrogen in the volume of the NiTi SMA and the thermo-mechanical aspect of the nucleation and growth of martensitic bands. For lower diffused hydrogen contents in the archwire, after loading and unloading with an imposed strain rate of 10⁻⁴ s⁻¹, an embrittlement is detected during the martensite transformation [22,31]. Furthermore, this embrittlement is detected for the imposed deformation at the beginning and the middle of the plateau of the austenite-martensite transformation and not at the end of the plateau of the austenite transformation. This behavior is attributed to the generation of a large density of dislocations during the applied cyclic strain, which can represent preferential sites for hydrogen diffusion. Therefore, this trapped hydrogen may cause difficulty for the martensite transformation.

It has been reported in many investigations that immediately after hydrogen charging with a high current density or for a long time of immersion, the absorbed hydrogen is more located in the subsurface of the archwire rather than the center [26]. This latter behavior is characterized by an increase in the hardness of the cross section and a typical fragile surface fracture in the affected

zone [22,32]. In several alloys like Ti-based [33] and austenitic steel [34,35], the dissolved hydrogen expands the crystal lattice of the parent phase, causing a distortion that gives rise to a series of changes in physical properties. Runciman et al. [36] inferred that the diffused hydrogen in austenite phase of the NiTi alloy would expand the volume of the alloy and affect its transformation temperature. Moreover, P. Rozenak et al. [37] mentioned that after releasing a high quantity of hydrogen out of austenitic steel, cracks would be present on the surface which had been in contact with the charging solution.

This paper aims to investigate the effect of strain rates on the mechanical behavior of the superelastic NiTi SMA after immersion for 6h and hydrogen diffusion. In the first part of the paper, the experimental procedure is presented, and the results are discussed with emphasis on the interaction between the trapped hydrogen in the archwire and the evolution of martensite variants. The goal of this part is to study the sensitivity of the superelastic Ni-Ti alloy to the strain rate after hydrogen-charging and loading and unloading. Indeed, this is due to the fact that during the removal and the reinsertion in the oral cavity by the orthodontist, the archwire may be subject to many cyclic loadings.

In the second part of the paper, preliminary research investigates the mechanical behavior after the desorption of the diffused high amount of hydrogen. The objective of latter part is to study the possibility of the reutilization of the archwire in the oral cavity after a few months of use in severe environments.

2. Materials and Methods

A Ni50.8Ti49.2 superelastic SMA with a cross section of $0.43 \times 0.64 \text{ mm}^2$ and a gage length of 20 mm was considered in this study (Figure 1). A Differential Scanning Calorimeter (DSC) (National Engineering School of Sousse, Sousse, Tunisia) was used in order to determine the transformation temperatures of the alloy at a scan rate of $10 \text{ }^\circ\text{C}/\text{min}$. The measured start and finish martensite transformation temperatures were, respectively: $M_s = -9 \text{ }^\circ\text{C}$ and $M_f = -32 \text{ }^\circ\text{C}$. Likewise, the start and finish austenite transformations were respectively: $A_s = -11 \text{ }^\circ\text{C}$ and $A_f = -3 \text{ }^\circ\text{C}$. The cyclic tension loading, from 1 to 50 cycles at room temperature, was applied. The applied monotonic and cyclic loading were done with strain rates of 10^{-4} and 10^{-2} s^{-1} using an Instron tensile 5966-type machine (National Engineering School of Sousse, Sousse, Tunisia) with a load cell of 10 kN. 10^{-4} and 10^{-2} s^{-1} represented the range of transition strain rate from superelastic to brittle material [28]. The stress-strain curves for the applied cyclic tensile test were performed with an imposed strain of 7.6%. To study the effect of hydrogen on the mechanical behavior, the superelastic NiTi archwires were polished with 1000-grit SiC paper and cleaned with acetone, then cathodically charged by immersion in an aqueous 0.9% NaCl solution. Specimens were charged with a current density of $10 \text{ A}/\text{m}^2$ for 6 h using a direct current power supply and a platinum anode, then annealed for 24 h at room temperature [21].

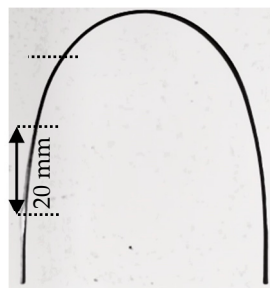


Figure 1. Specimen length of the as-received orthodontic wire.

To study the mechanical behavior of the NiTi arc wire after hydrogen desorption an annealing was done at $400 \text{ }^\circ\text{C}$ for one hour. Table 1 summarizes the type of tested specimens at different imposed strain rates. Hardness tests were conducted at room temperature after hydrogen charging and annealing under an applied load of 0.98 N for 15 s. Scanning electron microscope observations utilizing a JEOL JSM-5400 microscope (ETAP, Tunis, Tunisia) were made to investigate the fracture surfaces

of the annealed specimens. After hydrogen charging for 6 h and annealing at room temperature for one day, the amount of absorbed hydrogen was measured. A gas chromatograph calibrated with a standard mixture of hydrogen and argon gases was used. Thermal desorption analysis (TDA) was done in vacuum at 10^{-6} Pa for the detection of hydrogen. Sampling was performed at 30-s intervals at a heating rate of 100 °C/h until reaching 500 °C. Specimens were cut into 20-mm segments and subjected to ultrasonic cleaning with acetone for 5 min. The segments were dried and measured. The starting time of hydrogen TDA was carried out after 10 min of drying.

Table 1. Type of tested specimens at different imposed strain rates.

Imposed Strain Rate	Type of Specimen		
10^{-4} s^{-1}	As received	Hydrogen charged and aged	Hydrogen charged, aged and annealed
10^{-2} s^{-1}	As received	Hydrogen charged and aged	Hydrogen charged, aged and annealed

3. Results and Discussion

3.1. Strain Rate Effect

Figure 2 shows typical stress-strain curves for tensile tests until the fracture of the studied Ni-Ti superelastic SMA at two strain rates. These strain rates correspond to the extension rates of 10^{-2} s^{-1} and 10^{-4} s^{-1} . For the low strain rate of 10^{-4} s^{-1} , an elastic deformation of the parent phase is observed, followed by the “plateau” of the austenite-martensite transformation at an almost constant load of 350 MPa, and then by an elastic deformation of the martensite phase. The critical yield stress of the starting martensite transformation is defined as the intersection of the double tangent method between the elastic part of the austenite transformation and the pseudo-plateau of the martensite transformation. Before any fracture, the martensite phase is plastically deformed; once this step is reached, the NiTi wire will lose its superelasticity. However, for the higher strain rates of 10^{-2} s^{-1} , the critical stress is about 400 MPa and a strain hardening effect of the austenite-martensite transformation plateau is detected.

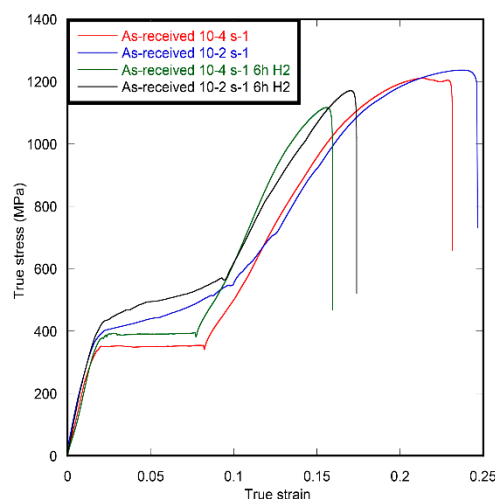


Figure 2. True tensile curve of as-received specimens, charged for 6 h with current density of 10 A/m^2 and aged at room temperature at strain rates of 10^{-4} s^{-1} and 10^{-2} s^{-1} .

The increase in the critical tensile stress and the slope of the austenite-martensite transformation for the higher strain rate is attributed to the fact that the higher the strain rate is applied, the less is the time to transfer the latent heat caused by the local self-heating of the domain front, and also the finer the variants of the martensite. Based on the above scenario, since the heat is not transferred away quickly from the numerous domain fronts, the temperature of the specimen goes up. As a result, the

needed applied stress for introducing new martensite variants becomes higher and the slope of the plateau of the martensite transformation increases [25,38]. Nevertheless, for the slow strain rate, the latent heat is evacuated and the number of variant interfaces is reduced. In addition, during the stress plateau, characterizing the austenite-martensite transformation, the applied load results in the growth of the limited number of variants, not to the nucleation of new ones [39,40].

After hydrogen charging in NaCl 0.9% with a current density of 10 A/m² for 6 h and ageing for 24 h at room temperature, the critical stress of the starting austenite-martensite transformation goes up from 350 MPa to 385 MPa with 10⁻⁴ s⁻¹ and to about 430 MPa with 10⁻² s⁻¹ of strain rates. Besides, the material keeps its superelastic behavior, and no embrittlement is detected.

Moreover, the critical stress for introducing the first variants of the martensite grows, compared to the applied tensile tests with the same strain rate for the non-charged samples. This rise in the value of the critical stress is attributed to the effect of diffused hydrogen after charging and ageing, which acts as an obstacle for the nucleation of the first martensite variants [7,27].

To illustrate the effect of mechanical loading and unloading during the use of the superelastic NiTi archwire, strain cycling is carried out until reaching the value of 7.6%. This value corresponds to the end of the stress plateau describing the austenite-martensite phase transformation. Figure 3a shows the true stress-strain curves under cyclic tensile loading-unloading with an imposed 7.6% strain of the as-received wire at a strain rate of 10⁻⁴ s⁻¹. In this figure, a decrease in the critical yield is noticed for the starting martensite transformation with an increase in the number of cycles. Indeed, the yield stress goes down from 350 MPa at the first cycle and reaches the value of 270 MPa after 50 cycles. In addition, the hardening-like slope of the pseudo-plateau progressively grows during cycling. These results go with the reduction in the size of the plateau of the austenite martensite by about 1%. Additionally, the hysteresis loops decrease constantly, with a decline in the reversibility effect of the superelasticity of the austenite-martensite phases.

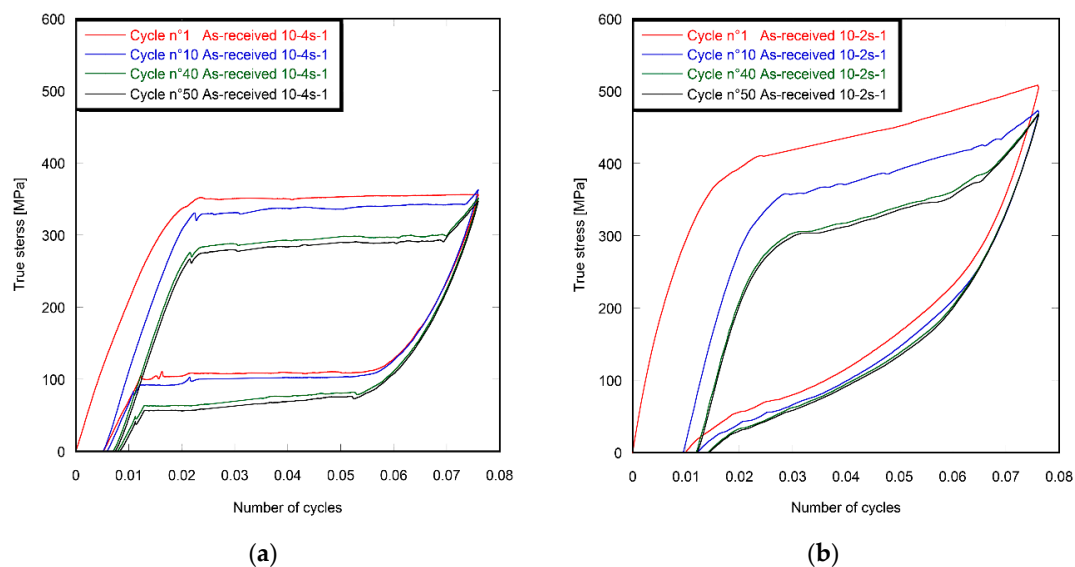


Figure 3. Tensile stress-strain curves with imposed strain rate of 10⁻⁴ s⁻¹ of (a) as-received and (b) hydrogen charged for 6 h and aged superelastic NiTi Shape Memory Alloy.

Figure 3b depicts the stress-strain curves under cyclic tensile loading-unloading with an imposed strain rate of 10⁻² s⁻¹ at room temperature. As indicated, these results show a similar behavior of the loaded and unloaded specimens with the 10⁻⁴ s⁻¹ strain rate. Nonetheless, the critical stress for the starting martensite transformation decreases from 400 MPa at the first cycle to 270 MPa at the 50th cycle. Besides, a rise in the residual deformation is noted at zero stress versus the number of cycles (Figure 4). These values are higher than the ones obtained after cycling with an imposed deformation of 10⁻⁴ s⁻¹.

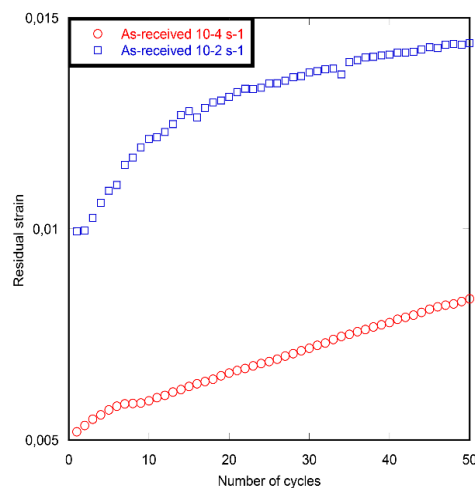


Figure 4. Residual strain rates at zero stress as a function of number of cycles of as-received specimen with imposed strain rates of 10^{-4} s^{-1} and 10^{-2} s^{-1} .

According to O. Ammar et al. [41], the residual strain at zero stress is caused by the generation of dislocations during the austenite martensite transformation and to a nontransformed martensite during the reverse transformation after unloading. However, with the strain rates of 10^{-2} s^{-1} , the temperature of the specimen goes up during loading, and the number of martensite variants is higher. Consequently, on the one hand, the needed stress to produce the martensite phase increases, which leads to the generation of a higher density of dislocations. On the other hand, since the number of martensite bands is big, the probability to obtain the nontransformed martensite at zero stress is high.

After hydrogen charging with a current density of 10 A/m^2 for 6 h at room temperature, the loading and unloading tensile curves with an imposed strain rate of 10^{-2} s^{-1} shows that the NiTi wire keeps its superelasticity (Figure 5a). Yet, the residual strain at zero stress rises with the increase in the number of cycles. In addition, these values are higher than those of the as-received and cycled NiTi alloy (Figure 5b). This behavior is observed in all cycles, and the difference between the obtained residual strain for the charged and non-immersed specimen grows in relation to the number of cycles. This result highlights that after hydrogen charging and cycling with an imposed strain rate of 10^{-2} s^{-1} , the more the number of cycles goes up, the more the NiTi progressively loses its superelasticity.

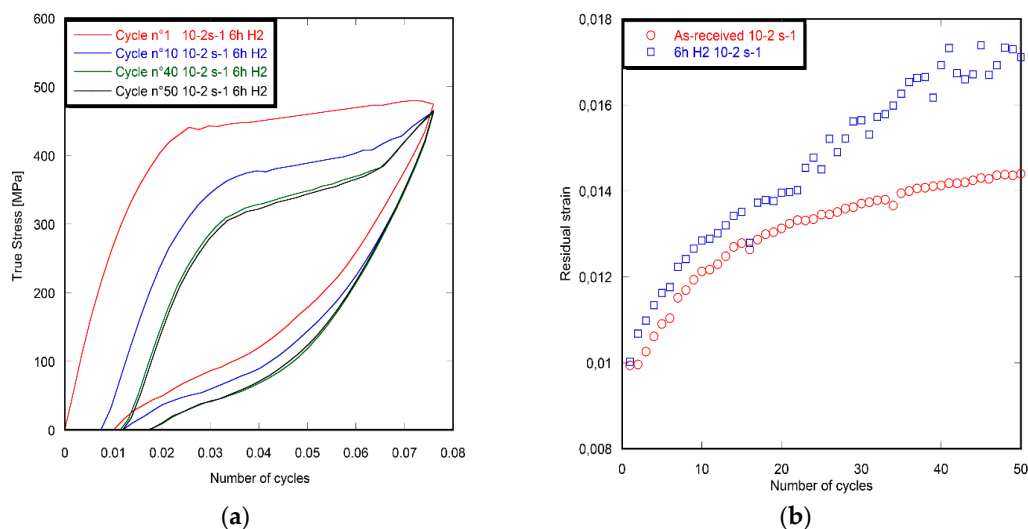


Figure 5. After 6 h of hydrogen charging and ageing (a) tensile loading and unloading with imposed strain rate of 10^{-2} s^{-1} and (b) evolution of residual strain at zero stress as a function of number of cycles.

For specimens charged by hydrogen for 6 h, aged for 24 h in air and cycled at room temperature with a lower strain rate of 10^{-4} s^{-1} (Figure 6a), a fracture occurs in brittle manner after 18 cycles. This premature failure is detected during loading, precisely in the plateau of the austenite-martensite transformation. These results are consistent with those obtained with the monotonic tensile test [28]. To explain the sensitivity of the NiTi alloy to the strain rate, an assumption based on the nucleation and growth of the martensite bands is given. Indeed, during low strain rates, the applied stress leads to the nucleation of a small number of variants that grow in the plateau of the martensite transformation. Nevertheless, after immersion, the diffused hydrogen acts as a barrier for the growth of the martensite bands, and embrittlement occurs. Contrarily, when the strain rate exceeds 10^{-3} s^{-1} , the applied stress tends to generate a large number of thin bands instead of having growing existing variants. Hence, the diffused hydrogen does not affect the superelasticity of the NiTi alloy.

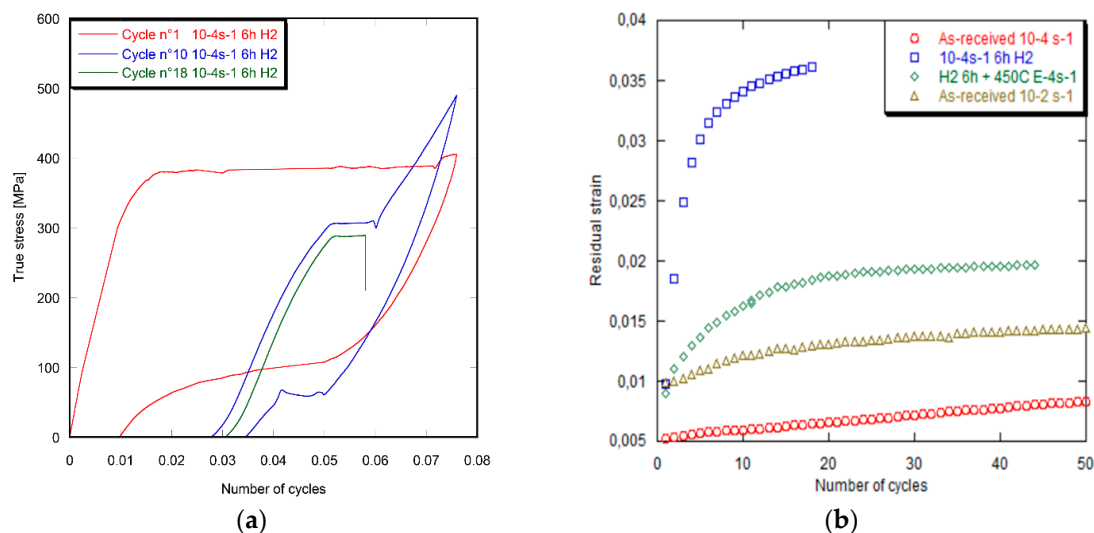


Figure 6. After 6 h of hydrogen charging and ageing (a) tensile loading and unloading with imposed strain rate of 10^{-4} s^{-1} and (b) evolution of residual strain at zero stress with number of cycles.

In comparison to the as-received specimen with an imposed strain of 10^{-4} s^{-1} , it is clear that the measured values of the residual strain at zero stress go up after immersion and ageing. Added to that, these values are even higher than the cycled alloy with an imposed strain rate of 10^{-2} s^{-1} (Figure 6b). For example, in the 17th cycle, this value is about 1.4% for the charged and cycled specimen with 10^{-2} s^{-1} , but it rises to 3.4% after immersion and cycling with an imposed strain of 10^{-4} s^{-1} . This result demonstrates that hydrogen plays a significant role in the embrittlement of the NiTi alloy when the applied strain rate is low.

Figure 7 shows the evolution of the dissipated energy density versus the number of cycles. This energy is defined as the area enclosed by loading and unloading curves for each cycle. It is indicated that before the fracture of the hydrogen charged and aged specimen with an imposed strain rate of 10^{-4} s^{-1} , the values of the dissipated energy density plummet, compared to the as-received sample (Figure 7a). This energy drops from $1.7 \times 10^7 \text{ J/m}^3$ at the first cycle to only $6 \times 10^6 \text{ J/m}^3$ after 15 cycles. However, for an imposed strain of 10^{-2} s^{-1} , an interesting behavior appears, which is marked by the fact that there is almost no difference between the dissipated energy density of the immersed and aged specimen and the dissipated energy density of the as-received NiTi archwire without hydrogen charging (Figure 7b). C. Morin et al. [42] mentioned that the dissipative energy in the polycrystalline NiTi was based mainly on the reversible transition from the austenite phase to the martensite structure. This transformation is characterized by the nucleation and growth of micro-domains at the level of grain sizes, leading to localized release or absorption of the latent heat during the forward or reverse phase transition process. Additionally, during the austenite-martensite

transformation, the propagation of the front of the martensite domains under loading causes an upsurge in the temperature at the interface as a result of the released latent and dissipative heats [43]. This behavior is assumed to be the same during the reverse transformation, where the absorption of the latent heat is caused by the front propagation of the austenite phase.

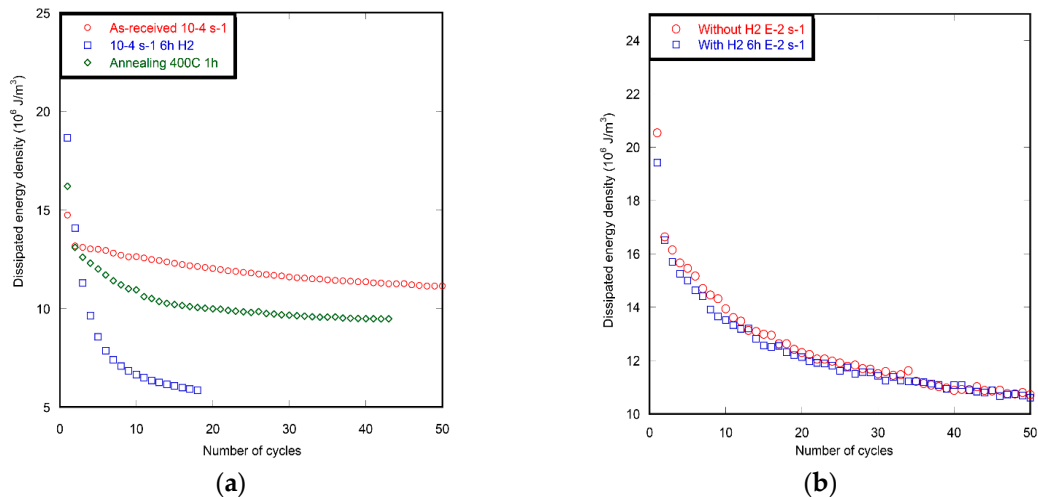


Figure 7. Evolution of dissipated energy density as a function of number of cycles of as-received and hydrogen charged specimen with imposed strain rate of (a) 10^{-4} s^{-1} and (b) 10^{-2} s^{-1} .

In our case, for a low strain rate of 10^{-4} s^{-1} , a significant loss in the dissipate energy density of the immersed and aged specimens as a function of the number of cycles is noticed, compared to the as-received archwires. This phenomenon is likely due to the transformation in the pseudo-plateau, which is based on the nucleation of a small number of martensite bands that grow under a constant load. After immersion, the diffused hydrogen acts as an obstacle against the growth of the martensite variants, and then the transformation becomes more difficult. Consequently, the density of the generated dislocations in the pseudo-plateau rises, which can explain the increase in the residual strain at zero stress and later the embrittlement after a small number of cycles. Besides, the absorbed hydrogen reduces the progress of the martensite bands, which are the main elements for causing the release of the latent heat. Afterwards, the dissipative energy density decreases as a function of the number of cycles.

Concerning the cycled specimen with a higher strain rate of 10^{-2} s^{-1} , similar values of the calculated dissipative energy density are noted, in all stages of cycling, between as-received and hydrogen-charged NiTi wires. Indeed, this behavior can be explained by the fact that when the strain rate is high, narrow martensite bands be obtained. Therefore, during the tensile test, the applied load does not affect the growth of the martensite variants, but it contributes to the generation of new ones. Hence, after immersion, the absorbed quantity of hydrogen has no effect on the mechanical behavior of the superelastic NiTi archwire during cycling, so there is no difference between specimens charged and non-charged by hydrogen. On the other hand, the increase in the residual strain could be the result of the multiplication of the number of dislocations as a function of the number of cycles, because this defect rises with the upsurge of the austenite-martensite fronts obtained with a high value of the applied load.

3.2. Annealing Effect

To evacuate the diffused hydrogen after medical use and enhance the mechanical properties of the archwires affected by hydrogen, TDA is performed on an immersed specimen in the NaCl 0.9% solution for 6 h and aged for 24 h at room temperature (Figure 8). The main objective of this heat treatment is to check whether we can reuse the arc wire diffused by hydrogen, after desorption.

The thermal desorption curve of hydrogen appears with a desorption peak at 320 °C. The progress of hydrogen entry into the alloy is shown as an increase in the total desorbed hydrogen, defined as the integrated peak intensity. In the as-received specimen, the amount of desorbed hydrogen, which corresponds to the initial concentration of hydrogen, is about 7 ppm. However, for the immersed and aged sample, the total amount of desorbed hydrogen in the whole volume is 668 ppm. This result indicates that after heating the charged specimen at 400 °C, most of the absorbed quantity of hydrogen will be released.

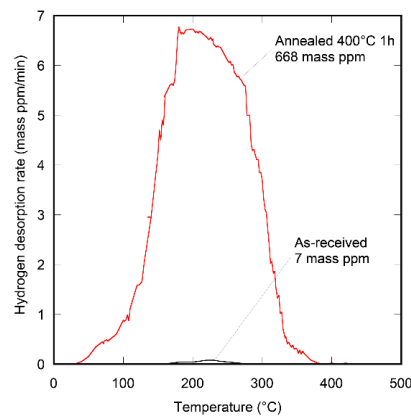


Figure 8. Hydrogen thermal desorption curves of immediately charged by hydrogen for 6 h at current density of 10 A/m² and aged for 24 h at room temperature.

The monotonic tensile test demonstrates that there is almost the same stress-strain curve between the as-received and annealed NiTi SMAs. After loading and unloading with an imposed strain rate of 10⁻⁴ s⁻¹, the annealed specimen is marked by a superelastic behavior, similar to the as-received one. Nonetheless, in the last cycles, and precisely at the 44th one, an embrittlement occurs (Figure 9). In addition, before fracture, the residual strains at zero stress are less than the obtained values after hydrogen charging, and are higher than those measured for the as-received samples (Figure 6b). Furthermore, after hydrogen desorption, the dissipated energy density versus the number of cycles shows a degradation of the superelasticity of the alloy. Indeed, from the first to the 44th cycles, the dissipated energy densities are, for all cases of the imposed strain rate of 10⁻⁴ s⁻¹, below the obtained values of the cycled as-received archwire (Figure 7a). This result highlights that the annealed material encounters some difficulties to nucleate and grow into martensite bands.

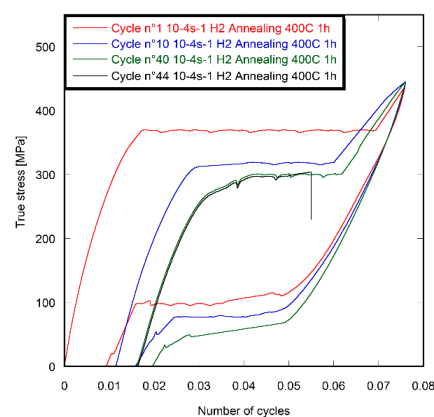


Figure 9. Tensile loading and unloading of annealed specimen for 1 h at 400 °C after immersion and ageing.

Figure 10 illustrates the Vickers microhardness depth profiles of the as-received NiTi alloys, the ones annealed at 400 °C for 1 h, and the ones charged by hydrogen for 6 h and aged for 24 h.

The hardness of the as-received specimen is almost constant in the entire cross section and is equal to about 360 Hv. For the immersed and aged specimen, the hardness is higher in the first 80 μm near the surface, and it converges to a stabilized value of about 400 Hv. This latter value is higher than the hardness of the alloy non-charged by hydrogen. This phenomenon is attributed to the fact that after 6 h of immersion, hydrogen is more localized in the subsurface rather than the center of the wire [23]. After ageing for 24 h at room temperature, the hydrogen diffuses in the whole volume of the archwire and affects the hardness of the entire specimen. However, after annealing for 1 h at 400 $^{\circ}\text{C}$, the Vickers hardness is similar to the hydrogen-charged sample for the first 80 μm from the surface. After that, it decreases to almost the same value of the as-received alloy. These results indicate that despite the desorption of hydrogen, the microstructure near the surface of the NiTi archwire is affected by the diffusion of hydrogen.

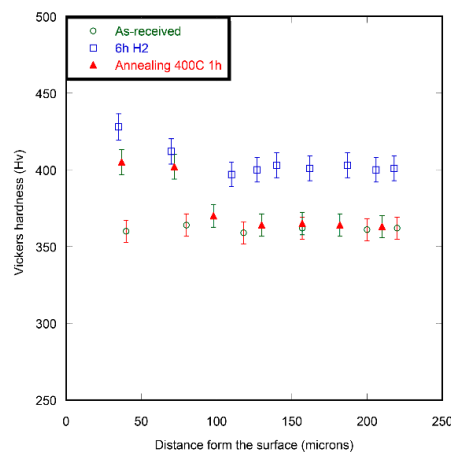


Figure 10. Linear pattern Vickers hardness from the surface to the center of as-received, immersed and aged, and annealed specimens after hydrogen diffusion.

The SEM observations of the fracture surfaces of the sample charged by hydrogen for 6 h with a current density of 10 A/m^2 , aged for 24 h and annealed for 1 h at 400 $^{\circ}\text{C}$ shows a typical ductile fracture, noticed by a necking (Figure 11a). Nonetheless, the magnification done on this surface indicates the existence of two zones: the inner zone marked by classic ductile deep dimples (Figure 11b), and the outer part with about 80 μm from the surface characterized by small dimples and almost flat surfaces (Figure 11c). This zone is the one that was in contact with the NaCl 0.9% solution during immersion, and where the concentration of hydrogen before ageing was higher [23]. These observations demonstrate that even after annealing, the microstructure of the immersed NiTi alloys is affected near the surface.

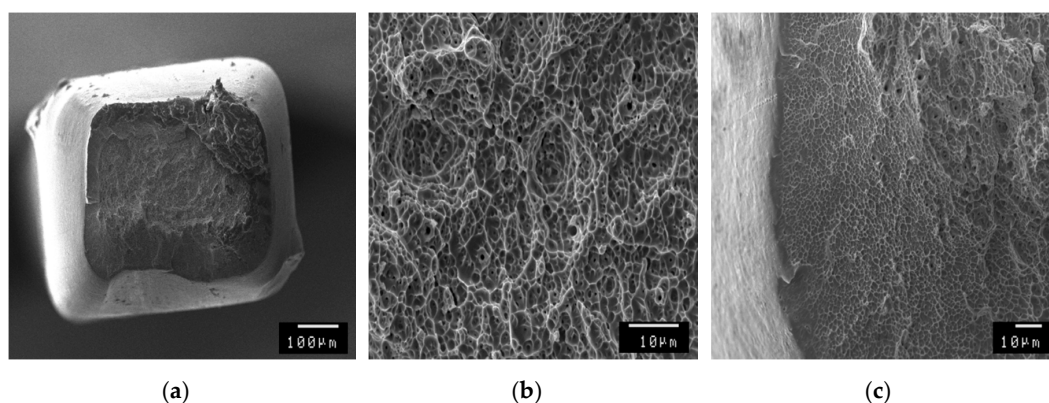


Figure 11. Scanning Electron Microscope images of typical fracture surfaces of annealed specimen: (a) general view; magnified views of (b) center parts and (c) outer part of specimen.

For austenitic steel, P. Rozenak et al. [33,44,45] showed that the absorption of supersaturated hydrogen could provide internal stress inducing a significant driving force for the formation of cracks. In addition, after electrochemical charging and ageing at room temperature, the X-ray diffraction reflection results indicated that the large amount of absorbed hydrogen led to a significant expansion of the hexagonal lattice of the austenite phase [46–48]. In fact, after SEM observations of AISI 316 austenitic stainless steel, no crack or martensite structure was found or could be clearly identified after the electrochemical charging and aging process. However, both hydrogen penetrations during emersion and hydrogen egress during aging were diffusion-controlled processes and a large amount of hydrogen concentration gradients in the surface layer, at depths comparable with the depth of X-ray penetration, was obtained experimentally. According to the X-ray analysis, these nonuniform distribution of hydrogen concentration in the austenitic structure conducted to the non-uniform expansion of the atomic microstructure, which led to the development of internal stresses and cracks. Moreover, these results were consistent with the calculation, based on the second Fick's law and Vegard's law [49] during the ingress and the egress of hydrogen, which showed that these compression stresses were 20 time higher than the ultimate tensile strength of the AISI type 316 stainless steel. Consequently, the formation and growth of surface cracks during the hydrogen release process at room temperature [37].

In an almost similar condition of the in situ stress relaxation of the NiTi SMA, the austenite-martensite transformation was obtained by the expansion of the volume of the alloy rather than the austenite-martensite transformation itself. Consequently, for our specimen charged by hydrogen and annealed for 1 h at 400 °C, the increase in the hardness near the sub-surface can be due to the expansion of the parent phase and the localized internal stress, hence the cracks after hydrogen desorption. Furthermore, this could be the main factor behind the growth of the dislocation density and the non-transformed martensite leading to the rise in the residual strain at zero stress as a function of the number of cycles. Likewise, the localized internal stress causing cracks after hydrogen desorption may cause the embrittlement of the archwire after 44 cycles, since the crack in the cyclic tests are probably initiated from the surface. Concerning the stress-strain curve, a similarity between the tensile test of the as-received specimen and the alloy charged by hydrogen and annealed is found. This behavior might be due to the fact that the tensile test depends only on the entire volume of the specimen, not to the surface. The effect of the amount of the diffused hydrogen on the cyclic tensile test after annealing will be studied in future work.

4. Conclusions

The results found in this study can be summarized as follows:

1. After 6 h of hydrogen charging with a current density of 10 A/m² and ageing, the cyclic tensile curves of the superelastic Ni–Ti SMA strongly depends on the strain rate. An embrittlement is detected in the 18th cycle for the imposed lower strain rate of 10^{−4} s^{−1}. However, there is no embrittlement detected for the higher strain rate of 10^{−2} s^{−1}. In addition, the dissipated energy density is tumbled for the low strain rate, compared to the as-received specimen. In contrast, no difference is detected for the higher strain rate. This behavior is attributed to the interaction between the hydrogen diffused into the volume and the thermo-mechanical mechanism of the nucleation and growth of the martensitic bands. This interaction is considered as strongly linked to the hydrogen diffused into the volume of the archwire and to the applied strain rates.
2. Despite the annealing of the NiTi archwire for 1 h at 400 °C, causing the desorption of the diffused hydrogen, the material is fractured in a brittle manner in the plateau of the austenite-martensite transformation after 44 cycles of loading and unloading. This result is attributed to the development of internal stress in the subsurface of the parent phase during hydrogen charging and to the creation of cracks and local zones of plasticity after desorption.

Author Contributions: Data curation, writing original draft, R.S. and F.G.; Methodology, T.H. and A.K.; Supervision, writing review and editing, A.A. and F.G.

Funding: This research and the APC were funded by the Deanship of Scientific Research, King Khalid University (KKU), Abha-Asir, Saudi Arabia, with grant number (R.G.P.1/69/40) under research groups program.

Acknowledgments: The authors extend their appreciation to the Deanship of Scientific Research at King Khalid University for funding this work through research groups program under grant number (R.G.P.1/69/40).

Conflicts of Interest: The authors declare no conflict of interest.

References

- Herget, G.; Müllner, M.; Suck, J.B.; Schmidt, R.; Wipf, H. Phonon Spectra of the Memory Alloy NiTi. *Europhys. Lett.* **1989**, *10*, 49–54. [[CrossRef](#)]
- Waitz, T.; Kazykhanov, V.; Karnthaler, H.P. Martensitic phase transformations in nanocrystalline NiTi studied by TEM. *Acta Mater.* **2004**, *52*, 137–147. [[CrossRef](#)]
- Sharma, N.; Jangra, K.; Raj, T. Applications of Nickel-Titanium Alloy. *J. Eng. Technol.* **2015**, *5*, 1. [[CrossRef](#)]
- Castleman, L.S.; Motzkin, S.M.; Alicandri, F.P. Biocompatibility of nitinol alloy as an endotracheal implant material. *J. Biomed. Mater. Res.* **1976**, *10*, 695–731. [[CrossRef](#)] [[PubMed](#)]
- Bhargava, R.R.; Verma, P.R. Strip-electro-mechanical yield model for transversely situated two semi-permeable collinear cracks in piezoelectric strip. *Theor. Appl. Fract. Mech.* **2016**, *81*, 32–49. [[CrossRef](#)]
- Lagoudas, D.C. *Shape Memory Alloys: Modeling and Engineering Applications*; Springer-Verlag: Berlin, Germany, 2008.
- Sarraj, R.; Letaief, W.E.; Hassine, T.; Gamaoun, F. Modeling of rate dependency of mechanical behavior of superelastic NiTi alloy under cyclic loading. *Int. J. Adv. Manuf. Technol.* **2019**, *100*, 2715–2724. [[CrossRef](#)]
- Petrini, L.; Migliavacca, F. Biomedical Applications of Shape Memory Alloys. *J. Metall.* **2011**, *2011*, 501483. [[CrossRef](#)]
- Bartzela, T.N.; Senn, C.; Wichelhaus, A. Load-deflection characteristics of superelastic nickel-titanium wires. *Angle Orthod.* **2007**, *77*, 991–998. [[CrossRef](#)] [[PubMed](#)]
- Bewerse, C.; Gall, K.R.; McFarland, G.J.; Zhu, P.; Brinson, L.C. Local and global strains and strain ratios in shape memory alloys using digital imagecorrelation. *Mater. Sci. Eng. A* **2013**, *568*, 134–142. [[CrossRef](#)]
- Eaton-Evans, J.; Dulieu-Barton, J.M.; Little, E.G.; Brown, I.A. A New Approach to Stress Analysis of Vascular Devices Using High Resolution Thermoelastic Stress Analysis. *Appl. Mech. Mater.* **2009**, *5–6*, 63–70. [[CrossRef](#)]
- Delpueyo, D.; Balandraud, X.; Grédiac, M. Applying infrared thermography to analyse martensitic microstructures in a Cu–Al–Be shape-memory alloy subjected to a cyclic loading. *Mater. Sci. Eng. A* **2011**, *528*, 8249–8258. [[CrossRef](#)]
- Helbert, G.; Saint-Sulpice, L.; Chirani, S.A.; Dieng, L.; Lecompte, T.; Calloch, S.; Pilvin, P. Experimental characterisation of three-phase NiTi wires under tension. *Mech. Mater.* **2014**, *79*, 85–101. [[CrossRef](#)]
- Brinson, L.C.; Schmidt, I.; Lammering, R. Stress-induced transformation behavior of a polycrystalline NiTi shape memory alloy: Micro and macromechanical investigations via in situ optical microscopy. *J. Mech. Phys. Solids* **2004**, *52*, 1549–1571. [[CrossRef](#)]
- Dayananda, G.N.; Rao, M.S. Effect of strain rate on properties of superelastic NiTi thin wires. *Mater. Sci. Eng. A* **2008**, *486*, 96–103. [[CrossRef](#)]
- Nemat-Nasser, S.; Guo, W.-G. Superelastic and cyclic response of NiTi SMA at various strain rates and temperatures. *Mech. Mater.* **2006**, *38*, 463–474. [[CrossRef](#)]
- Tobushi, H.; Shimeno, Y.; Hachisuka, T.; Tanaka, K. Influence of strain rate on superelastic properties of TiNi shape memory alloy. *Mech. Mater.* **1998**, *30*, 141–150. [[CrossRef](#)]
- Letaief, W.E.; Hassine, T.; Gamaoun, F. In situ stress relaxation mechanism of a superelastic NiTi shape memory alloy under hydrogen charging. *Philos. Mag. Lett.* **2017**, *97*, 50–57. [[CrossRef](#)]
- Huang, H.-H.; Chiu, Y.H.; Lee, T.H.; Wu, S.C.; Yang, H.W.; Su, K.H.; Hsu, C.C. Ion release from NiTi orthodontic wires in artificial saliva with various acidities. *Biomaterials* **2003**, *24*, 3585–3592. [[CrossRef](#)]
- Mirjalili, M.; Momeni, M.; Ebrahimi, N.; Moayed, M.H. Comparative study on corrosion behaviour of Nitinol and stainless steel orthodontic wires in simulated saliva solution in presence of fluoride ions. *Mater. Sci. Eng. C* **2013**, *33*, 2084–2093. [[CrossRef](#)] [[PubMed](#)]

21. Lee, T.-H.; Wang, C.-C.; Huang, T.-K.; Chen, L.-K.; Chou, M.-Y.; Huang, H.-H. Corrosion resistance of titanium-containing dental orthodontic wires in fluoride-containing artificial saliva. *J. Alloys Compd.* **2009**, *488*, 482–489. [[CrossRef](#)]
22. Gamaoun, F.; Skhiri, I.; Bouraoui, T.; Zineb, T.B. Hydrogen effect on the austenite-martensite transformation of the cycled Ni-Ti alloy. *J. Intell. Mater. Syst. Struct.* **2014**, *25*, 980–988. [[CrossRef](#)]
23. Gamaoun, F.; Ltaief, M.; Bouraoui, T.; Zineb, T.B. Effect of hydrogen on the tensile strength of aged Ni-Ti superelastic alloy. *J. Intell. Mater. Syst. Struct.* **2011**, *22*, 2053–2059. [[CrossRef](#)]
24. Yokoyama, K.; Tomita, M.; Sakai, J. Hydrogen embrittlement behavior induced by dynamic martensite transformation of Ni-Ti superelastic alloy. *Acta Mater.* **2009**, *57*, 1875–1885. [[CrossRef](#)]
25. Yokoyama, K.; Watabe, S.; Hamada, K.; Sakai, J.; Asaoka, K.; Nagumo, M. Susceptibility to delayed fracture of Ni-Ti superelastic alloy. *Mater. Sci. Eng. A* **2003**, *341*, 91–97. [[CrossRef](#)]
26. Yokoyama, K.; Ogawa, T.; Takashima, K.; Asaoka, K.; Sakai, J. Hydrogen embrittlement of Ni-Ti superelastic alloy aged at room temperature after hydrogen charging. *Mater. Sci. Eng. A* **2007**, *466*, 106–113. [[CrossRef](#)]
27. Gamaoun, F.; Hassine, T. Ageing effect and rate dependency of a NiTi shape memory alloy after hydrogen charging. *J. Alloy Compd.* **2014**, *615*, s680–s683. [[CrossRef](#)]
28. Gamaoun, F.; Hassine, T.; Bouraoui, T. Strain rate response of a Ni-Ti shape memory alloy after hydrogen charging. *Philos. Mag. Lett.* **2014**, *94*, 30–36. [[CrossRef](#)]
29. Letaief, W.E.; Hassine, T.; Gamaoun, F. Rate Dependency During Relaxation of Superelastic Orthodontic NiTi Alloys After Hydrogen Charging. *Shape Mem. Superelasticity* **2016**, *2*, 121–127. [[CrossRef](#)]
30. Letaief, W.E.; Hassine, T.; Gamaoun, F. A coupled model between hydrogen diffusion and mechanical behavior of superelastic NiTi alloys. *Smart Mater. Struct.* **2017**, *26*, 075001. [[CrossRef](#)]
31. Sarraj, R.; Hassine, T.; Gamaoun, F. Mechanical behavior of NiTi arc wires under pseudoelastic cycling and cathodically hydrogen charging. *Mater. Res. Express* **2018**, *5*, 015704. [[CrossRef](#)]
32. Yokoyama, K.; Kaneko, K.; Ogawa, T.; Moriyama, K.; Asaoka, K.; Sakai, J. Hydrogen embrittlement of work-hardened Ni-Ti alloy in fluoride solutions. *Biomaterials* **2005**, *26*, 101–108. [[CrossRef](#)] [[PubMed](#)]
33. Rozenak, P.; Eliezer, D. Phase changes related to hydrogen-induced cracking in austenitic stainless steel. *Acta Metall.* **1987**, *35*, 2329–2340. [[CrossRef](#)]
34. Gustiono, D.; Sakaguchi, N.; Shibayama, T.; Kinoshita, H.; Takahashi, H. Plane and Cross-Sectional TEM Observation to Clarify the Effect of Damage Region by Ion Implantation on Induced Phase Transformation in Austenitic 301 Stainless Steel. *Mater. Trans.* **2004**, *45*, 65–68. [[CrossRef](#)]
35. Xu, X.; Wang, L.; Yu, Z.; Hei, Z. A comparative study on microstructure of the plasma-nitrided layers on austenitic stainless steel and pure Fe. *Surf. Coat. Technol.* **2005**, *192*, 220–224.
36. Runciman, A.; Chen, K.C.; Pelton, A.R.; Trépanier, C. Effects of Hydrogen on the Phases and Transition Temperatures of NiTi. *Int. Conf. Shape Mem. Superelastic Technol.* **2006**, 185–196. [[CrossRef](#)]
37. Rozenak, P.; Loew, A. Stress distributions due to hydrogen concentrations in electrochemically charged and aged austenitic stainless steel. *Corros. Sci.* **2008**, *50*, 3021–3030. [[CrossRef](#)]
38. Tomita, M.; Yokoyama, K.; Asaoka, K.; Sakai, J. Hydrogen thermal desorption behavior of Ni-Ti superelastic alloy subjected to tensile deformation after hydrogen charging. *Mater. Sci. Eng. A* **2008**, *476*, 308–315. [[CrossRef](#)]
39. He, Y.J.; Sun, Q.P. Macroscopic equilibrium domain structure and geometric compatibility in elastic phase transition of thin plates. *Int. J. Mech. Sci.* **2010**, *52*, 198–211. [[CrossRef](#)]
40. He, Y.J.; Sun, Q.P. Rate-dependent domain spacing in a stretched NiTi strip. *Int. J. Solids Struct.* **2010**, *47*, 2775–2783. [[CrossRef](#)]
41. Ammar, O.; Dieng, L.; Haddar, N. Modeling of strain rate effect on the pseudoelastic behavior of NiTi SMA using a simple thermomechanical coupling model. *Mech. Mater.* **2018**, *124*, 7–17. [[CrossRef](#)]
42. Morin, C.; Mourni, Z.; Zaki, W. Thermomechanical coupling in shape memory alloys under cyclic loadings: Experimental analysis and constitutive modeling. *Int. J. Plast.* **2011**, *27*, 1959–1980. [[CrossRef](#)]
43. Zhang, X.; Feng, P.; He, Y.; Yu, T.; Sun, Q. Experimental study on rate dependence of macroscopic domain and stress hysteresis in NiTi shape memory alloy strips. *Int. J. Mech. Sci.* **2010**, *52*, 1660–1670. [[CrossRef](#)]
44. Rozenak, P.; Zevin, L.; Eliezer, D. Hydrogen effects on phase transformations in austenitic stainless steels. *J. Mater. Sci.* **1984**, *19*, 567–573. [[CrossRef](#)]
45. Rozenak, P.; Zevin, L.; Eliezer, D. Internal stresses in austenitic steels cathodically charged with hydrogen. *J. Mater. Sci. Lett.* **1983**, *2*, 63–66. [[CrossRef](#)]

46. Gavriljuk, V.G.; Hänninen, H.; Tarasenko, A.V.; Tereshchenko, A.S.; Ullakko, K. Phase transformations and relaxation phenomena caused by hydrogen in stable austenitic stainless steels. *Acta Metall. Mater.* **1995**, *43*, 559–568. [[CrossRef](#)]
47. Rozenak, P.; Bergman, R. X-ray phase analysis of martensitic transformations in austenitic stainless steels electrochemically charged with hydrogen. *Mater. Sci. Eng. A* **2006**, *437*, 366–378. [[CrossRef](#)]
48. Narita, N.; Altstetter, C.J.; Birnbaum, H.K. Hydrogen-related phase transformations in austenitic stainless steels. *Metall. Trans. A* **1982**, *13*, 1355–1365. [[CrossRef](#)]
49. Goodier, J.N. The thermal stress in a strip due to variation of temperature along the length and through the thickness. *J. Appl. Phys.* **1936**, *7*, 156–159. [[CrossRef](#)]



© 2019 by the authors. Licensee MDPI, Basel, Switzerland. This article is an open access article distributed under the terms and conditions of the Creative Commons Attribution (CC BY) license (<http://creativecommons.org/licenses/by/4.0/>).